Supplementary Information for Non-Gaussian diffusion near surfaces

A. Alexandre*, M. Lavaud*, N. Fares, E. Millan, Y. Louyer, T. Salez, Y. Amarouchene, T. Guérin and D.S. Dean

I. THEORETICAL FORMALISM

A. Cumulants of the horizontal displacement

The fourth cumulant is obtained by direct computation:

$$\langle X_t^4\rangle_{\rm c} \equiv \langle X_t^4\rangle - 3\langle X_t^2\rangle^2 = 12\int_0^t {\rm d}s \int_0^t {\rm d}s' \ \left[\langle D_\parallel(Z_s)D_\parallel(Z_{s'})\rangle - \langle D_\parallel(Z_s)\rangle\langle D_\parallel(Z_{s'})\rangle\right], \tag{S1}$$

where we have used Wick's theorem. The translational invariance in the x direction means that all odd cumulants are zero. The cumulant can be rewritten as

$$\begin{aligned}\langle X_t^4\rangle_{\rm c} &= 12\int_0^t {\rm d}s \int_0^t {\rm d}s' \left\langle \left[D_\parallel(Z_s) - \left\langle D_\parallel(Z_s)\right\rangle\right]\left[D_\parallel(Z_{s'}) - \left\langle D_\parallel(Z_{s'})\right\rangle\right]\right\rangle, \\ &= 12\left\langle \left\{\int_0^t {\rm d}s \ \left[D_\parallel(Z_s) - \left\langle D_\parallel(Z_s)\right\rangle\right]\right\}^2\right\rangle.\end{aligned} \tag{S2}$$

The latter equation has the same Kubo-type structure as the second cumulant in the Taylor dispersion problem [1]. Interestingly, from the last expression in Eq. (S2), we see that $\langle X_t^4\rangle_{\rm c}$ takes always positive values, regardless of the expression of $D_\parallel(z)$.

To proceed, we introduce the propagator $p(z|z';t)$, *i.e.* the probability to go from z' at time zero to z at time t, for the process Z_t. The propagator obeys:

$$\frac{\partial p(z|z';t)}{\partial t} = -\mathcal{H}\ p(z|z';t), \tag{S3}$$

where the operator $\mathcal{H}$ acts on the variable z, and is given by Eq. (1) of the main text, with the initial condition $p(z|z';0) = \delta(z-z')$. In this framework, for the process X_t, when Z_t starts from equilibrium, one has:

$$\langle X_t^4\rangle_{\rm c} = 24\int_0^t {\rm d}s \int_0^s {\rm d}s' \ \int_{-H}^H {\rm d}z\, D_\parallel(z) \int_{-H}^H {\rm d}z' D_\parallel(z')\left[p(z|z';s-s') - p_0(z)\right]p_0(z'). \tag{S4}$$

We now introduce the left and right eigenfunctions, respectively $\psi_{{\rm L}\lambda}$ and $\psi_{{\rm R}\lambda}$, of $\mathcal{H}$ which obey:

$$\mathcal{H}^\dagger\psi_{{\rm L}\lambda} = \lambda\psi_{{\rm L}\lambda}, \qquad\qquad \mathcal{H}\psi_{{\rm R}\lambda} = \lambda\psi_{{\rm R}\lambda}, \tag{S5}$$

with λ the associated eigenvalue and $\mathcal{H}^\dagger$ the adjoint operator of $\mathcal{H}$, which is in general not self-adjoint. The solution of Eq. (S3) for $p(z|z';t)$ then has the decomposition:

$$p(z|z';t) = \sum_\lambda \psi_{{\rm R}\lambda}(z)\psi_{{\rm L}\lambda}(z')\exp(-\lambda t). \tag{S6}$$

The right eigenfunctions satisfy the no-flux boundary condition:

$$\left\{D_\perp(z)\left[\frac{{\rm d}\psi_{{\rm R}\lambda}}{{\rm d}z} + \beta V'(z)\psi_{{\rm R}\lambda}(z)\right]\right\}_{z=\pm H} = 0, \tag{S7}$$

and one can show [2] that the left eigenfunctions satisfy the Neumann condition: $\frac{\rm d}{{\rm d}z}\psi_{{\rm L}\lambda}(z)|_{z=\pm H} = 0$. The eigenfunctions corresponding to $\lambda = 0$ can be written as: $\psi_{{\rm R}0}(z) = p_0(z)$ and $\psi_{{\rm L}0}(z) = 1$, so that they respect the normalization condition $\int {\rm d}z\, \psi_{{\rm R}0}(z)\psi_{{\rm L}0}(z) = 1$. Using this representation of $p(z|z';t)$ in the Kubo formula of Eq. (S4), the fourth cumulant can be rewritten as:

$$\langle X_t^4\rangle_{\rm c} = 24\int_{-H}^H {\rm d}z \int_{-H}^H {\rm d}z'\, D_\parallel(z)D_\parallel(z')p_0(z')\sum_{\lambda>0}\left[\frac{t}{\lambda} - \frac{1}{\lambda^2} + \frac{\exp(-\lambda t)}{\lambda^2}\right]\psi_{{\rm R}\lambda}(z)\psi_{{\rm L}\lambda}(z'), \tag{S8}$$

which is Eq. (9) of the main text. In principle, Eq. (S8) can be computed explicitly if the relevant eigenfunctions and eigenvalues are known, however in most cases, they are not known explicitly. Nevertheless, they can still be computed numerically using standard numerical packages and thus used to predict the full temporal behavior of $\langle X_t^4 \rangle_{\rm c}$. In contrast, the short-time and long-time behaviors can be extracted analytically from Eq. (S8), as explained in the following subsection.

B. Asymptotic behavior of the fourth cumulant

In the limit where $t \to 0$, Eq. (S8) simplifies to:

$$\langle X_t^4 \rangle_{\rm c} \underset{t\to 0}{\simeq} 12\, t^2 \int_{-H}^{H} {\rm d}z \int_{-H}^{H} {\rm d}z' D_\parallel(z) D_\parallel(z') p_0(z') \sum_{\lambda>0} \psi_{{\rm R}\lambda}(z) \psi_{{\rm L}\lambda}(z'). \tag{S9}$$

Furthermore, the completeness relation leads to:

$$\sum_{\lambda>0} \psi_{{\rm R}\lambda}(z) \psi_{{\rm L}\lambda}(z') = \delta(z-z') - p_0(z). \tag{S10}$$

Then, Eq. (S9) becomes:

$$\left\langle X_t^4 \right\rangle_{\rm c} \underset{t\to 0}{\simeq} 12\, t^2 \left[\left\langle D_\parallel^2 \right\rangle_0 - \left\langle D_\parallel \right\rangle_0^2 \right]. \tag{S11}$$

The short-time behavior of the fourth cumulant is thus quadratic in time, and is proportional to the variance of $D_\parallel$ with respect to the equilibrium measure.

The fourth cumulant can also be computed in the limit where $t \to \infty$, *i.e.* for $t \gg \lambda_1^{-1}$, where λ_1 is the first non-zero eigenvalue of $\mathcal{H}$. This is done by using a formulation in terms of Green's functions [3, 4], which can be shown to be intimately linked to the macro-transport theory [5]. In this case, Eq. (S8) simplifies to:

$$\langle X_t^4 \rangle_{\rm c} \underset{t\to +\infty}{\simeq} 24 \left(D_4 t - C_4 \right), \tag{S12}$$

with

$$D_4 = \int_{-H}^{H} {\rm d}z \int_{-H}^{H} {\rm d}z' D_\parallel(z) D_\parallel(z') p_0(z') \sum_{\lambda>0} \frac{\psi_{{\rm R}\lambda}(z) \psi_{{\rm L}\lambda}(z')}{\lambda}, \tag{S13}$$

and

$$C_4 = \int_{-H}^{H} {\rm d}z \int_{-H}^{H} {\rm d}z' D_\parallel(z) D_\parallel(z') p_0(z') \sum_{\lambda>0} \frac{\psi_{{\rm R}\lambda}(z) \psi_{{\rm L}\lambda}(z')}{\lambda^2}. \tag{S14}$$

Using the method described in [1] (see Section III. A therein), we obtain:

$$D_4 = \left\langle \frac{\left[J(z) e^{\beta V(z)} \right]^2}{D_\perp(z)} \right\rangle_0, \qquad J(z) = \int_{-H}^{z} {\rm d}z' \exp[-\beta V(z')] [D_\parallel(z') - \langle D_\parallel \rangle_0]. \tag{S15}$$

This form is particularly useful to carry out numerical computations with arbitrary potentials and diffusion tensors. One can also show that:

$$C_4 = \left\langle R^2 \right\rangle_0 - \langle R \rangle_0^2, \qquad R(z) = \int_{-H}^{z} {\rm d}z' \, \frac{J(z') \exp\left[\beta V(z')\right]}{D_\perp(z')}. \tag{S16}$$

C. Analytical solutions for narrow channels

In this part, we consider the simple case where there is no potential and where the channel has a sufficiently narrow width with respect to the particle size so that the diffusion constant can be taken to vary quadratically within the channel:

$$D_\perp(z) = D_{\perp 0} \left(1 - \frac{z^2}{H^2} \right), \; D_{||}(z) = D_{||0} \left(1 - \frac{z^2}{H_{\rm s}^2} \right), \tag{S17}$$

where H_s a characteristic length that can be considered as a diffusive slip length when $H_s > H$ and $D_\perp$ vanishes at $z = \pm H$. The coefficients $D_{\perp 0}$ and $D_{||0}$ depend on the effective channel height H and a. The quadratic model of the diffusion constant in the height direction has been proposed in a theoretical context by a number of authors [6, 7]. In Fig. S1(b), we have compared the superposition approximation for the local components of the diffusion tensor to simple quadratic fits for a narrow channel, as one might expect, due to the narrowness of the channel this approximation works fairly well.

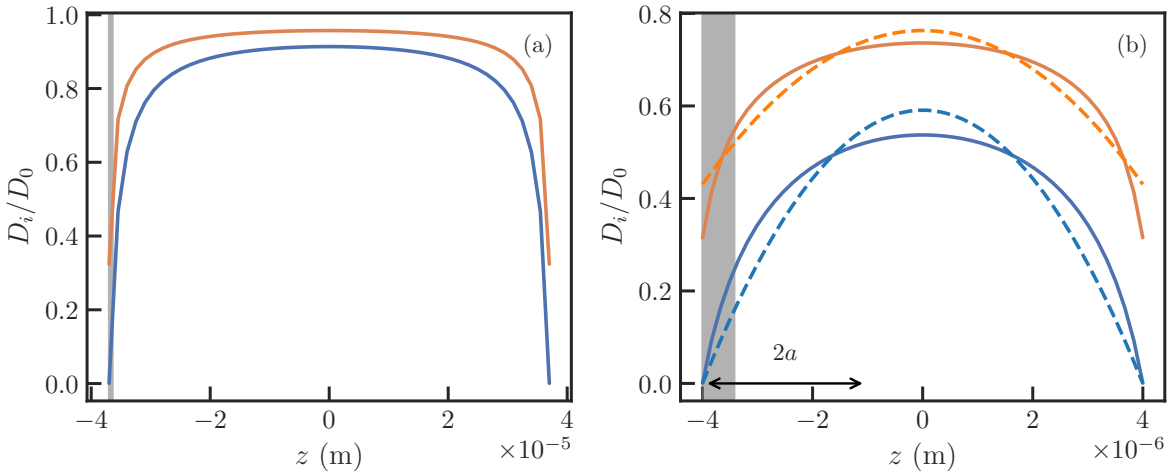

FIG. S1: (a) Perpendicular and parallel diffusion coefficients, $D_\perp$ (blue) and $D_{||}$ (orange), as functions of vertical coordinate z, for a channel width $H_p = H + a = 40$ μm, in the superposition approximation (see Eq. (S51)), using the parameters of the experiment. The grey region has width l_B and represents the region where the particle remains typically localized due to gravity. (b) Same as previous panel, appart from the value of the width, which is $H_p = H + a = 5.5$ μm. We also show here the quadratic approximations to $D_\perp$ and $D_{||}$ (dashed orange and blue lines). The arrow represents the diameter $2a$ of the bead.

In the absence of an external potential, one has $p_0(z) = (2H)^{-1}$ and the effective longitudinal diffusion constant is given by:

$$\langle D_{||} \rangle_0 = D_{||0} \left(1 - \frac{H^2}{3H_s^2} \right). \tag{S18}$$

Using Eqs. (S15,S16), we find:

$$D_4 = \frac{2D_{||0}^2 H^6}{135 D_{\perp 0} H_s^4}, \; C_4 = \frac{D_{||0}^2 H^8}{405 D_{\perp 0}^2 H_s^4}. \tag{S19}$$

Since the diffusivities show quadratic profiles, a more detailed analysis, involving full time dependence is available. In fact, here the operator $\mathcal{H}$ (see Eq. (1)) is self adjoint and its eigenvalues and normalized eigenfunctions are given by:

$$\psi_n(z) = \sqrt{\frac{2n+1}{2H}} \, P_n\left(\frac{z}{H}\right), \qquad \lambda_n = \frac{D_{||0}}{H^2} n(n+1), \tag{S20}$$

where P_n denotes the n^{th} degree Legendre polynomial.

If we write $D_{||}(z)$ in terms of Legendre polynomials, we get:

$$\frac{D_{||}(z)}{D_{||0}} = \left(1 - \frac{H^2}{3H_s^2} \right) P_0\left(\frac{z}{H}\right) - \frac{2H^2}{3H_s^2} P_2\left(\frac{z}{H}\right). \tag{S21}$$

From Eq. (S8), the full time dependent behavior of the fourth cumulant is then given by:

$$\frac{\langle X_t^4 \rangle_c}{24} = \frac{2D_{||0}^2 H^6}{135 D_{\perp 0} H_s^4} t - \frac{D_{||0}^2 H^8}{405 D_{\perp 0}^2 H_s^4} \left[1 - \exp\left(-\frac{6 D_{\perp 0} t}{H^2} \right) \right], \tag{S22}$$

which is Eq. (15) in the main text. From the latter, one can recover the late time corrections given in Eq. (S19). This solution of the fourth cumulant can be extended to arbitrary expressions of $D_{||}$ as long as it can be expressed on the basis of Legendre polynomials:

$$D_{||}(z) = \sum_{n=0}^{\infty} d_n P_n\left(\frac{z}{H}\right), \qquad d_n = \frac{2n+1}{2}\int_{-1}^{1} \mathrm{d}\zeta\ P_n(\zeta) D_{||}(\zeta H). \tag{S23}$$

The fourth cumulant reads in this general case:

$$\frac{\langle X_t^4\rangle_{\mathrm{c}}}{24} = \sum_{n\geq 1}\left[\frac{H^2}{D_{\perp 0} n(n+1)}t - \frac{H^4}{D_{\perp 0}^2 n^2(n+1)^2} + \frac{H^4 e^{-\frac{D_{\perp 0}}{H^2}n(n+1)t}}{D_{\perp 0}^2 n^2(n+1)^2}\right]\frac{d_n^2}{2n+1}. \tag{S24}$$

D. Probability distribution function of lateral displacement

The probability distribution function (PDF) of the displacement X_t can be analysed by considering the corresponding cumulant generating function:

$$g(q,t) = \langle e^{qX_t}\rangle = \left\langle e^{q\int_0^t \sqrt{2D_{||}(Z_s)}dB_{x,s}}\right\rangle = \left\langle e^{q^2\int_0^t D_{||}(Z_s)ds}\right\rangle, \tag{S25}$$

where in the last equality we have averaged over the Brownian increments $dB_{x,s}$ which are independent of Z_s. This has the form of a functional of the process Z_s:

$$g(\mu,t) = \left\langle e^{\mu\int_0^t u(Z_s)ds}\right\rangle, \tag{S26}$$

where $\mu = q^2$ and $u(z) = D_{||}(z)$. Written this way, we see the mathematical resemblance between the diffusing diffusivity problem and Taylor dispersion in a velocity field $u(z)$:

$$Y_t = \int_0^t u(Z_s)ds, \tag{S27}$$

at the level of the generating functions of the two processes. The cumulant generating function, by definition, yields the cumulants of Y_t via

$$g(\mu,t) = \exp\left[\sum_{n=1}^{\infty}\frac{\mu^n}{n!}\langle Y_t^n\rangle_c\right]. \tag{S28}$$

The functional $g(\mu,t)$ can be evaluated by using the Feynman-Kac formula [8] as $g(\mu,t) = \langle G(\mu,t,z)\rangle_0$, where G satisfies the equation:

$$\frac{\partial G(\mu,t,z)}{\partial t} = [-\mathcal{H}^\dagger + \mu D_{\|}(z)]G(\mu,t,z), \qquad G(\mu,t=0,z) = 1. \tag{S29}$$

Similar equations appear for the diffusion of anisotropic objects [9, 10]. If one determines the eigenvalues $\lambda(\mu)$ of $\mathcal{H}^\dagger - \mu D_{\|}(z)$, then we obtain:

$$g(\mu,t) = \sum_{\lambda(\mu)} e^{-\lambda(\mu)t}\int_{-H}^{H} dz\ p_0(z)\phi_{\mathrm{R},\lambda}(z)\int_{-H}^{H} dz'\ \phi_{\mathrm{L},\lambda}(z'), \tag{S30}$$

where $\phi_{\mathrm{R},\lambda}, \phi_{\mathrm{L},\lambda}$ are respectively the right and left eigenfunctions of $\mathcal{H}^\dagger - \mu D_{\|}(z)$.

At late times, the solution is dominated by the smallest eigenvalue $\lambda_0(\mu)$ of the operator $\mathcal{H}^\dagger - \mu D_{\|}(z)$:

$$g(\mu,t) = e^{-\lambda_0(\mu)t}\int_{-H}^{H} dz\ p_0(z)\phi_{\mathrm{R},0}(z)\int_{-H}^{H} dz'\ \phi_{\mathrm{L},0}(z'), \tag{S31}$$

where

$$\mathcal{H}^\dagger\phi_{\mathrm{R},0}(z) - \mu D_{\|}(z)\phi_{\mathrm{R},0}(z) = \lambda_0(\mu)\phi_{\mathrm{R},0}(z). \tag{S32}$$

Note that the prefactor is obtained from the initial condition $g(t,\mu,0)=1$. Comparing with the definition (S28) of the cumulants via the generating function, this result then implies that at late times:

$$-\lambda_0(\mu)t=\sum_{n=1}^{\infty}\frac{\mu^n}{n!}\langle Y_t^n\rangle_c. \tag{S33}$$

This formula means that all cumulants of Y_t (and also all cumulants of X_t) scale as t for large times:

$$\langle Y_t^n\rangle_{\rm c}\underset{t\to\infty}{\simeq}u_n t, \tag{S34}$$

and the coefficients u_n are found by considering the series expansion of $\lambda_0(\mu)$ near $\mu=0$, hence $u_n=-(\partial_\mu^n\lambda_0)_{\mu=0}$. This gives an alternative method of computing the late time behavior of the cumulants using perturbation theory and one can check that it agrees with the Kubo formula used in the Letter for the second and fourth cumulants.

E. Convergence to Gaussian statistics in the diffusive scaling regime.

The goal of this section is to establish how the PDF $p(x,t)$ converges to a Gaussian when $x=\xi\sqrt{t}$ (this, in the diffusive regime), in the large time limit. We notice that the Fourier transform of $p(x,t)$ written $\hat{p}(k,t)$ is obtained by setting $q=-ik$ in the moment generating function $[g(q,t)=\hat{p}(k,t)]$. Thus, p can be recovered by taking the inverse Fourier transform of g :

$$p\left(x=\xi\sqrt{t},t\right)=\frac{1}{2\pi}\int_{-\infty}^{\infty}dk\ e^{ik\xi\sqrt{t}}\hat{p}(k,t)=\frac{1}{2\pi\sqrt{t}}\int_{-\infty}^{\infty}d\tilde{k}\ e^{i\tilde{k}\xi}\ g\left(-i\frac{\tilde{k}}{\sqrt{t}},t\right), \tag{S35}$$

where we have set $\tilde{k}=k\sqrt{t}$ in the second equality. Now, we may formally use Eq.(S28) to write:

$$p\left(x=\xi\sqrt{t},t\right)=\frac{1}{2\pi\sqrt{t}}\int_{-\infty}^{\infty}d\tilde{k}\exp\left[i\tilde{k}\xi+\sum_{n=1}^{\infty}(-\tilde{k}^2)^n\frac{\langle Y_t^n\rangle_{\rm c}}{t^n n!}\right] \tag{S36}$$

$$\underset{t\to\infty}{\simeq}\frac{1}{2\pi\sqrt{t}}\int_{-\infty}^{\infty}d\tilde{k}\exp\left[i\tilde{k}\xi+\sum_{n=1}^{\infty}(-\tilde{k}^2)^n\frac{u_n t}{t^n n!}\right], \tag{S37}$$

where we have used the previously determined behavior $\langle Y^n\rangle_c\simeq u_n t$ at large times. We see that all terms with $n\geq 2$ in this expansion are proportional to t^{1-n} and can thus be treated as perturbative terms when $t\to\infty$. In particular, keeping only the term $n=2$ leads to:

$$p\left(x=\xi\sqrt{t},t\right)\underset{t\to\infty}{\simeq}\frac{1}{2\pi\sqrt{t}}\int_{-\infty}^{\infty}d\tilde{k}\ e^{i\tilde{k}\xi-u_1\tilde{k}^2}\left(1+\frac{u_2\tilde{k}^4}{2t}\right). \tag{S38}$$

Using $u_1=\langle D_{||}\rangle_0$ and $u_2=2D_4$ and performing the integral leads to:

$$p\left(x=\xi\sqrt{t},t\right)\underset{t\to\infty}{\simeq}\frac{1}{\sqrt{4\pi t\langle D_{||}\rangle_0}}\exp\left(-\frac{\xi^2}{4\langle D_{||}\rangle_0}\right)\left\{1+\frac{D_4}{16\ t\langle D_{||}\rangle_0^4}\left[12\langle D_{||}\rangle_0^2(1-\xi^2)+\xi^4\right]\right\}. \tag{S39}$$

The above derivation basically recovers the first terms of the Gram Charlier series of type A used in the analysis of non-Gaussian [11] random variables. We thus see that in the diffusive scaling regime, non-Gaussian statistics decay with time. This is of course compatible with the observation, made in the main text, that the non-Gaussianity parameter $\alpha(t)=\langle X_t^4\rangle_{\rm c}/\langle X_t^2\rangle_{\rm c}^2\sim 1/t$ at late times. In the next section, we will see that the only trace of non-Gaussian statistics at very late times is in the extreme value statistics where the central limit theorem does not apply.

F. Extreme value statistics

Here, we consider contributions to the PDF at large values of x corresponding to trajectories which diffuse much further than the typical (diffusive) ones. The probability of these rare events can be computed using large deviation theory. The reader is referred to [12] for a standard introduction written for physicists. If we consider the moment

generating function in the form of Eq. (S25), we see that for q large, paths which are highly dispersed dominate the functional. The large deviation analysis for Taylor dispersion was carried out in Refs. [13–15] and we adapt the analysis there to study the diffusing diffusivity model under consideration here.

The tails of the displacement PDF are obtained by analyzing the limit $q \to \infty$ in the moment generating function. We are sampling the large dispersion regime where Z_t stays close to z^* where $D_{||}(z)$ attains its maximum. We make the physically relevant assumption that that z^* is not located at the wall. We thus look for an eigenfunction $\phi_{\mathrm{R},0}$ that is localized near $z = z^*$. Writing $z = z^* + \frac{\zeta}{|q|^\alpha}$, for some $\alpha > 0$, the eigenvalue equation for $\phi_{\mathrm{R},0}(z) = \psi_0(\zeta)$ simplifies at leading order in $q \to \infty$:

$$\left\{ |q|^{2\alpha} D_\perp(z^*) \frac{d^2}{d\zeta^2} + \lambda_0(q) + q^2 \left[D_{||}(z^*) - \frac{1}{2} |D''_{||}(z^*)| \frac{\zeta^2}{|q|^{2\alpha}} \right] \right\} \psi(\zeta) = 0. \tag{S40}$$

We see that we have to take $\alpha = 1/2$ so that ψ does not depend on q. We recognize the quantum harmonic oscillator problem, so that we directly write the lowest eigenvalue solution:

$$\psi_0(\zeta) \propto \exp\left[-\sqrt{\frac{|D''_{||}(z^*)|}{8 D_\perp(z^*)}} \zeta^2 \right], \qquad \lambda_0(q) = |q| \sqrt{\frac{|D''_{||}(z^*)| D_\perp(z^*)}{2}} - q^2 D_{||}(z^*). \tag{S41}$$

If we assume the large deviation form of $p(x,t) \sim e^{-t f(x/t)}$ (up to exponential prefactors), we find that

$$g(q,t) \sim \int dx \; e^{-t f\left(\frac{x}{t}\right) + qx} \sim \int d\xi \; e^{t[q\xi - f(\xi)]} \sim \exp\left\{ \max_\xi [q\xi - f(\xi)] t \right\}, \tag{S42}$$

where we have used the saddle point method and the notation $\xi = x/t$. Since we already know that $g(q,t) \propto \exp[-t\lambda_0(q)]$, we see that

$$-\lambda_0(q) = \max_\xi [q\xi - f(\xi)]. \tag{S43}$$

Hence, the minimal eigenvalue $-\lambda_0(q)$ is the Legendre transform of the large deviation function f [13–15]. Inverting the Legendre transform we obtain:

$$f(\xi) = \max_q [q\xi + \lambda_0(q)]. \tag{S44}$$

The behavior of f for large x is obtained by taking the Legendre transform of $\lambda_0(q)$ for large $|q|$ given by Eq. (S41), this leads to:

$$f(\xi) \underset{|\xi| \to \infty}{=} \frac{1}{4 D_{||}(z^*)} \left[\xi + \mathrm{sign}(\xi) \sqrt{\frac{|D''_{||}(z^*)| D_\perp(z^*)}{2}} \right]^2 + \mathcal{O}(1), \tag{S45}$$

which is Eq. (21) in the main text. This means that the PDF of the displacement $p(x,t) \sim e^{-t f(x/t)}$ has the form of a shifted Gaussian, with a diffusivity given by the maximal value $D_{||}(z^*)$, however the weight of these paths is strongly suppressed by the way the Gaussian is centered.

Finally, the large deviation function for small ξ can be simply computed from the second moment and reads:

$$f(\xi) = \frac{\xi^2}{4 \langle D_{||} \rangle_0}. \tag{S46}$$

II. EXPERIMENTAL DETAILS

The experimental data presented in the main text corresponds to spherical polystyrene colloids of nominal radius 1.5 μm purchased from Polybead©. The ensemble of particles that are tracked have reached their equilibrium distribution due to the lag time between the insertion of the particles and the beginning of the measurement protocol. In the latter, a single sphere is three-dimensionally tracked using a self-calibrated interferometric method based on Mie Holography [16].

A previously-calibrated plane wave (wavelength 532 nm) illuminates a dilute colloidal suspension. The light scattered by a given particle interferes with the incident beam in the focal plane of a ×100-objective and the interference

pattern, called hologram, is magnified toward a CCD camera. Then, the strong dependencies of a hologram on both the physical properties and the position of the sphere lead to the precise measurement of the aforementioned characteristics. The first 10000 holograms are fitted to determine the physical properties of the sphere, namely its radius and optical index. Those physical properties are then set and all the holograms are fitted, leading to the trajectory of the sphere, and, after its statistical analysis, to the observables depicted in the main text.

The experimental equilibrium PDF p_0 shown in Fig. 2(a) of the main text is obtained by binning the z position of the sphere on a logarithmic normal grid.

The ensemble averages required in the computation of the experimental second and fourth cumulants (see Eqs. (6) and (7)) depicted in Fig. 2(c,d) of the main text, are obtained through sliding temporal averages, assuming ergodicity:

$$\langle X_t^n \rangle = \frac{1}{N} \sum_{j=0}^{N-1} \left[x(t+t_j) - x(t_j) \right]^n \equiv \frac{1}{N} \sum_{j=0}^{N-1} \left[\Delta x(t \,|\, t_j) \right]^n \ , \tag{S47}$$

where $n, N \in \mathbb{N}$, $x(t)$ is the x position of the sphere at time t, and where $t_j = j\, f_{\mathrm{a}}^{-1}$ with the frame rate $f_{\mathrm{a}} = 100$ Hz of the acquisition.

The experimental local diffusion coefficients depicted in Fig. 2(b) of the main text are obtained by a stochastic force inference algorithm [17]. An unbiased estimator $\hat{d}$ of the local diffusion coefficient in the x direction (the adaptation to the z direction being straightforward) is built as follows:

$$\hat{d}(t_j) = \frac{\left[\Delta x(\delta t \,|\, t_{j-1}) + \Delta x(\delta t \,|\, t_j) \right]^2}{4\delta t} + \frac{\Delta x(\delta t \,|\, t_{j-1}) \Delta x(\delta t \,|\, t_j)}{2\delta t} \ , \tag{S48}$$

where δt is a chosen multiple of f_a^{-1} and $\Delta x(\delta t \,|\, t_j)$ is the distance traveled by the sphere over a time δt and starting at t_j. Each of the above values of $\hat{d}$ corresponds to a given height $H + z$ and their distribution is estimated on a normal grid $\{\tilde{z}\}$ with a polynomial function basis of order 3: $\sum a_k(\tilde{z})(H+z)^k$, in which the a_k are real functions. The accuracy of the method is confirmed *a posteriori* by the agreement with the theoretical predictions, as shown in Fig. 2. We also note that the first term on the right-hand side of Eq. (S48) arises from the temporal linearity of the MSD (see Eq. (6) of the main text) while the second one is a correction that allows us to estimate accurately the local diffusion coefficients close to the surface ($H + z \leq 100$ nm) where the experimental data is scarce.

Finally, several observables that stem from the sphere's trajectory – which include the ones described above – depend on the physical parameters of the system, namely B, l_{D} and l_{B} defined in Eq. (16) of the main text. These parameters are thus fitted simultaneously to increase the method's precision.

III. NUMERICAL SIMULATIONS

We consider hereafter the three overdamped Langevin equations:

$$\begin{cases} \mathrm{d}X_t = \sqrt{2D_{\parallel}(Z_t)}\, dB_{x,t} \\ \mathrm{d}Y_t = \sqrt{2D_{\parallel}(Z_t)}\, dB_{y,t} \\ \mathrm{d}Z_t = D'_{\perp}(Z_t)dt - \beta D_{\perp}(Z_t) V'(Z_t) dt + \sqrt{2D_{\perp}(Z_t)}\, dB_{z,t} \ , \end{cases} \tag{S49}$$

where the first right-hand-side term of the last equation corresponds to the spurious force in the Ito convention, and where $dB_{x,t}$, $dB_{y,t}$ and $dB_{z,t}$ are independent Brownian increments. The simulation takes into account the bottom and top walls positioned at $\pm H_{\mathrm{p}}$. The potential $V(z)$ is given by Eq. (16) of the main text.

The effective viscosity perpendicular to a single wall is given by Eq. (18) of the main text. In the case of the relatively wide channel studied experimentally, we can use the superposition approximation and estimate the excess drag forces with respect to the bulk ones as the sum of the corresponding contributions from the individual surfaces. The total effective viscosities are thus given by:

$$\mu_i^T(z) - \mu_0 \simeq \mu_i^+(z) - \mu_0 + \mu_i^-(z) - \mu_0 \ , \tag{S50}$$

with $i \in \{\parallel, \perp\}$, and where $\mu_i^{\pm}(z)$ denote the individual effective viscosities near both walls. The Stokes-Einstein relation then gives:

$$D_i(z) \simeq \frac{k_{\mathrm{B}}T}{6\pi a \left[\mu_i^+(z) + \mu_i^-(z) - \mu_0 \right]} \ . \tag{S51}$$

We plot $D_{||}(z)$ and $D_{\perp}(z)$ for $H_{\rm p} = 40\mu$m in Fig. S1(a), and for $H_{\rm p} = 5.5\mu$m in Fig. S1(b). Also shown for comparison are the parabolic approximations for the narrow-channel case.

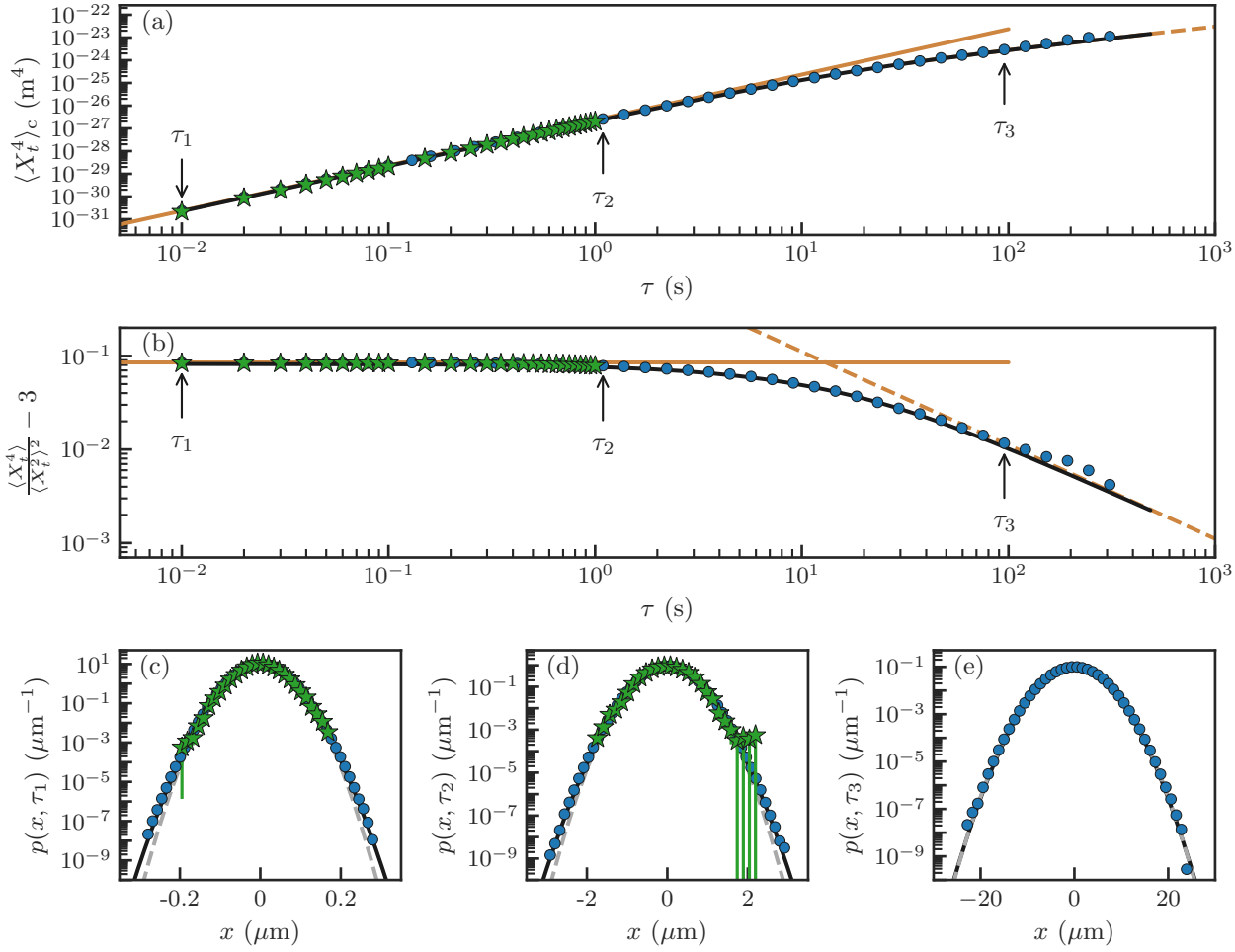

FIG. S2: Fourth cumulant (a), and rescaled fourth cumulant (b) as functions of time, for $H_{\rm p} = 40\,\mu$m. Green diamonds: experimental data. Blue circles: simulation data. Orange solid and dashed lines: asymptotic predictions (see main text). Solid black lines: exact theory at all times (see main text). The three last panels correspond to the PDF $p(x,t)$ for (c) $t = \tau_1 = 0.01$s, (d) $t = \tau_2 = 1.09$s and (e) $t = \tau_3 = 95.4$ s. Green diamonds: experimental data. Blue circles: simulation data. Grey dashed lines: Gaussian distribution. Solid black lines: exact prediction obtained by numerically inverting the Fourier transform $\hat{p}(k,t) = g(q = -ik, t)$ given by Eq. (S31).

We discretize Eq. (S49) by using an Euler scheme where solutions are approximated by $X_t(t) \approx X_n(t_n)$, $Y_t(t) \approx Y_n(t_n)$ and $Z_t(t) \approx Z_n(t_n)$, with $t_n = n\Delta t$, Δt being the simulation time step. The increments $dB_{k,t}$ ($k \in \{x, y, z\}$) are approximated by $\Delta B_{k,n} = W_{k,n}$, where W_{k_n} are independent Gaussian-distributed random variables of zero mean and unit variance. This leads to the discrete stochastic equations:

$$\begin{cases} X_{n+1} = X_n + \sqrt{2D_{\parallel}(Z_n)}\, W_{x,n}\sqrt{\Delta t} \\ Y_{n+1} = Y_n + \sqrt{2D_{\parallel}(Z_n)}\, W_{y,n}\sqrt{\Delta t} \\ Z_{n+1} = Z_n + D'_{\perp}(Z_n)\Delta t - \beta D_{\perp}(Z_n)V'(Z_n)\Delta t + \sqrt{2D_{\perp}(Z_n)}\, W_{z,n}\sqrt{\Delta t}\ . \end{cases} \tag{S52}$$

We numerically integrate (S52) with $\Delta t = 0.01$ s, for a total time of 1000 s, with identical physical parameters as the experimental ones. The system is allowed to first equilibrate in the vertical direction. From approximately 12 million trajectories, we extract the numerical fourth cumulant $\langle X_t^4\rangle_{\rm c}$ at all times using the PDF $p(x,\tau)$ of displacements $x = X_{t+\tau} - X_t$ generated from sliding temporal averaging. Specifically, the fourth cumulant is numerically calculated

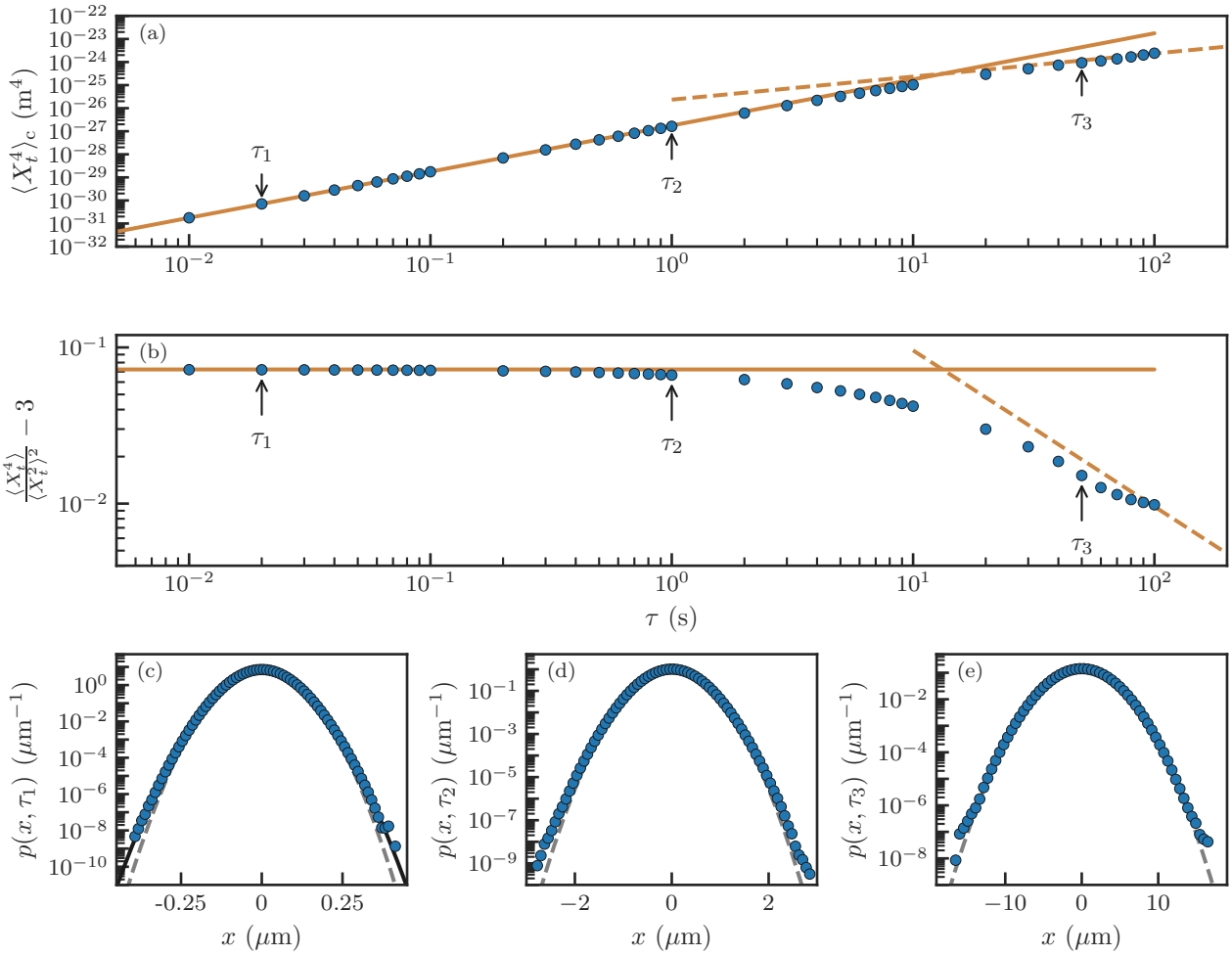

FIG. S3: Fourth cumulant (a), and rescaled fourth cumulant (b) as functions of time, for $H_\mathrm{p} = 5.5\,\mu$m. Green diamonds: experimental data. Blue circles: simulation data. Orange solid and dashed lines: asymptotic predictions (see main text). Solid black lines: exact theory at all times (see main text). The three last panels correspond to the PDF $p(x,t)$ for (c) $t = \tau_1 = 0.01$s, (d) $t = \tau_2 = 1.09$s and (e) $t = \tau_3 = 95.4$ s. Green diamonds: experimental data. Blue circles: simulation data. Grey dashed lines: Gaussian distribution. Solid black lines: exact prediction obtained by numerically inverting the Fourier transform $\hat{p}(k,t) = g(q = -ik, t)$ given by Eq. (S31).

from:

$$\langle X^4_{t=\Delta\tau}\rangle_\mathrm{c} = \int_{-\infty}^{+\infty} u^4 P(u,\Delta\tau)\,\mathrm{d}u - 3\left[\int_{-\infty}^{+\infty} u^2 P(u,\Delta\tau)\mathrm{d}u\right]^2 . \tag{S53}$$

Finally, as shown in Fig. 2(d) of the main text and in Fig. S2, the numerical results are in good agreement with both theoretical and experimental results, for a channel with $H_\mathrm{p} = 40\,\mu$m. We have also carried out numerical simulations for a much narrower channel, *i.e.* with $H_\mathrm{p} = 5.5\,\mu$m, but otherwise using the same parameters as the ones in the experimental setup. The results are shown in Fig. S3.

[1] Alexandre, A., Guérin, T. & Dean, D. S. Generalized Taylor dispersion for translationally invariant microfluidic systems. *Phys. Fluids* **33**, 082004 (2021).

[2] Gardiner, C. W. *Stochastic methods for physics, and handbook for the natural and social sciences* (Springer Series in Synergetics, 2009).

[3] Guérin, T. & Dean, D. S. Force-induced dispersion in heterogeneous media. *Phys. Rev. Lett.* **115**, 020601 (2015).

[4] Guérin, T. & Dean, D. S. Kubo formulas for dispersion in heterogeneous periodic nonequilibrium systems. *Phys. Rev. E* **92**, 062103 (2015).

[5] Brenner, H. & Edwards, D. A. *Macrotransport Processes* (Butterworth-Heinemann, 1993).

[6] Lau, A. W. & Lubensky, T. C. State-dependent diffusion: Thermodynamic consistency and its path integral formulation. *Phys. Rev. E* **76**, 011123 (2007).

[7] Avni, Y., Komura, S. & Andelman, D. Brownian motion of a charged colloid in restricted confinement. *Phys. Rev. E* **103**, 042607 (2021).

[8] Øksendal, B. *Stochastic differential equations* (Springer, New-York, 2003).

[9] Munk, T., Höfling, F., Frey, E. & Franosch, T. Effective perrin theory for the anisotropic diffusion of a strongly hindered rod. *EPL (Europhysics Letters)* **85**, 30003 (2009).

[10] Kurzthaler, C., Leitmann, S. & Franosch, T. Intermediate scattering function of an anisotropic active brownian particle. *Scientific reports* **6**, 1–11 (2016).

[11] Cramér, H. *Mathematical methods of statistics* (Princeton university press, 1946).

[12] Touchette, H. The large deviation approach to statistical mechanics. *Phys. Rep.* **478**, 1–69 (2009).

[13] Haynes, P. & Vanneste, J. Dispersion in the large-deviation regime. part 2. cellular flow at large péclet number. *J. Fluid Mech.* **745**, 351–377 (2014).

[14] Haynes, P. & Vanneste, J. Dispersion in the large-deviation regime. part 1: shear flows and periodic flows. *J. Fluid Mech.* **745**, 321–350 (2014).

[15] Kahlen, M., Engel, A. & Van den Broeck, C. Large deviations in taylor dispersion. *Phys. Rev. E* **95**, 012144 (2017).

[16] Lavaud, M., Salez, T., Louyer, Y. & Amarouchene, Y. Stochastic inference of surface-induced effects using brownian motion. *Phys. Rev. Res.* L032011 (2021). Publisher: APS.

[17] Frishman, A. & Ronceray, P. Learning force fields from stochastic trajectories. *Phys. Rev. X* **10**, 021009 (2020).